Coarsening kinetics of heteroepitaxial islands in nucleationless Stranski-Krastanov growth

P. Liu,[1] Y. W. Zhang,[2,*] and C. Lu[1]
[1]*Institute of High-Performance Computing, Singapore*
[2]*Department of Materials Science, National University of Singapore and Institute of Materials Research and Engineering, Singapore*
(Received 21 December 2002; published 1 July 2003)

A large-scale three-dimensional computer investigation of coarsening kinetics of heteroepitaxial islands during nucleationless Stranski-Krastanov growth is conducted. Both surface diffusion and condensation are considered. It is found that island formation and coarsening kinetics are strongly influenced by the growth rate and growth mode. Under the nucleationless growth mode, unusual coarsening kinetics, i.e., the superlinear increase in the mean island volume with respect to time, and the higher-than-linear-rate decrease in the areal density of islands with respect to time described by Floro *et al.* [Phys. Rev. Lett. **84**, 701 (2000)], is observed. It is proposed that unusual coarsening kinetics is attributed to the island volume distribution at the beginning of coarsening. The standard mean-field theory considering the island volume distribution at the beginning of coarsening reproduces the observed behavior.

DOI: 10.1103/PhysRevB.67.035402 PACS number(s): 68.55.−a, 68.35.Bs

INTRODUCTION

The self-assembly of quantum dots (QD's) through the Stranski-Krastanov (SK) growth mode has attracted a great deal of attention in recent years. Ideally if each island has the same size, shape, and composition, the dense array of epitaxial islands can be used for quantum dot applications due to unique optical, electronic, and magnetic properties.[1] During SK growth, the formation of QD's can occur through two routes: QD's can initiate by nucleation[2] or surface roughening (nucleationless),[3,4] followed by island growth and coarsening. The former usually gives rise to a wide range of island distribution as nucleation is a random process and therefore is ill-controlled, whereas the latter usually gives rise to a relatively more uniform and regular island array via the cooperative formation of the quantum dots.

Although enormous efforts have been made to achieve uniform and regular QD arrays through self-assembly, so far there is no reliable way to do so. The current uniformity and regularity of QD's is insufficient for majority of QD device applications. Therefore it is of interest to know the size distribution of QD's and how it evolves during growth.

Coarsening kinetics of self-assembled QD's can provide important information on the size distribution and evolution of QD's. Traditional understanding of QD coarsening kinetics is that coarsening of clusters follows Ostwald ripening, which involves a diffusion-mediated mass transfer from smaller to larger islands.[5–7] Ostwald ripening theories without considering mismatch strain have been well established.[8–10] Recently, it was found that island coarsening can be promoted by mechanisms other than Ostwald ripening. It is observed that (1) coarsening can be dominated by dynamic coalescence, which involves diffusion and subsequent coarsening of islands;[11] (2) coarsening can be promoted by static coarsening, where islands undergo coalescence only when neighboring islands touch;[2,12] and (3) coarsening can be driven by the Gibbs-Thomson effect, which favors larger-sized islands due to the lower vapor pressure around them. Smaller islands dissolve to establish a concentration gradient towards larger islands, which will continue to grow at the expense of smaller islands.[2,11]

During heteroepitaxial growth, the instability of surfaces under strain and subsequent island formation and coarsening is caused by the competition between the strain energy and the surface energy of the system. The instability of surfaces under strain was analyzed by Asaro and Tiller[13] and Grinfeld.[14] The origin of the instability is the reduction of the total free energy of the epitaxial system. However, the role of mismatch strain between the island layer and the substrate is still controversial. On one hand, it is observed that the island size distribution is consistent with that of homoepitaxial growth, implying that a strain-mediated mechanism is irrelevant.[15] The underlying argument is that although the mismatch strain does work to form three-dimensional (3D) islands, it is insufficiently large enough to control the shape of the islands and hence size distribution during growth. On the other hand, it is also believed that elastic interactions in a dense array of islands contribute significantly to the growth kinetics to reveal unusual coarsening kinetics,[2,16,17] which is inconsistent with the standard Ostwald ripening kinetics.

Computer simulations have been used to understand the formation and coarsening kinetics of epitaxial islands.[18–22] These simulations have revealed many details of the processes that occur during growth, such as cluster edge diffusion, adatom diffusion between clusters, and island nucleation and mobility. Most of the studies have focused on the first route of forming QD's, that is, through the sequence of nucleation, growth, and coalescence.[18–20] Although some modeling efforts[21,22] have been devoted to studying the second route of forming QD's, that is, through the sequence of surface roughening, formation of islands, growth, and ripening, due to the small number of islands involved, the coarsening kinetics revealed by these studies is not yet complete.

In this paper, we will study island formation and coarsening kinetics in the SK growth through large-scale computer simulations. Our attention is focused on the second route, that is, islands are formed through surface roughening rather than nucleation. Our simulations reveal many detailed pictures of island formation and coarsening kinetics. In particular, a bell-shaped island size distribution at the beginning of

coarsening is observed. It is found that the island size distribution can give rise to unusual coarsening kinetics, that is, the mean island volume increases superlinearly with time and the areal density of islands decreases at a higher-than-linear rate.[16] The standard mean field theory, with consideration of the bell-shaped island volume distribution at the beginning of coarsening, reproduces the observed behavior.

PROBLEM FORMULATION

Consider an elastically isotropic thin film with lattice spacing a_f heteroepitaxially grown on an elastically isotropic substrate with lattice spacing a_s. The mismatch strain is defined as $\varepsilon_0=(a_f-a_s)/a_s$. The substrate with thickness h_s is bonded to a rigid substrate. Although we consider heteroepitaxial growth in the present paper, for simplicity, we neglect the mismatch of elastic properties between the substrate and the film, i.e., the film and substrate have the same elastic properties.

At the film surface, mass diffusion and condensation are related to the magnitude of the surface chemical potential. If surface energy is isotropic and does not depend on surface strain, the surface chemical potential can be written as

$$\chi=\chi_0+\Omega(\omega-\kappa\gamma), \tag{1}$$

where χ_0 is the chemical potential of the bulk material, which is the reference chemical potential, Ω is the atomic volume of the diffusive atom, $\omega=\sigma_{ij}\varepsilon_{ij}/2$ is the strain energy density, κ is the mean curvature (the sum of two principal curvatures), and γ is the film surface energy. For simplicity, surface energy is assumed to be isotropic. For the film and the substrate, a linear elastic relation between the stress and strain is assumed, i.e., $\sigma_{ij}=C_{ijkl}\varepsilon_{kl}$, where C_{ijkl} is the component of elastic modulus tensor, σ_{ij} is the component of stress tensor, and ε_{kl} is the component of strain tensor.

The growth rate is proportional to the growth flux and the sticking coefficient.[23] The growth flux is dependent on the difference between the chemical potential of the vapor phase and the film surface. The larger the difference, the larger the growth flux.[23] To first-order accuracy, the condensation rate of the thin film surface, ν_g, is assumed to be proportional to the difference between the chemical potential of the vapor phase, $\chi_0+\chi_\nu$, and the surface chemical potential, χ, i.e.,

$$\nu_g=\eta(\chi_0+\chi_\nu-\chi), \tag{2}$$

where η is a growth parameter that depends on the sticking coefficient, temperature, and the mass of the vapor particle. Here, χ_ν is the relative chemical potential of the vapor phase.

Both surface diffusion and condensation contribute to the evolution of the film surface. Based on the conservation of mass, the surface evolution rate can be written as

$$\nu_n=D\nabla_s^2\chi+\eta(\chi_0+\chi_\nu-\chi), \tag{3}$$

where ν_n is the normal velocity, $D=D_s\delta_s/k_BT$, D_s is the surface diffusion coefficient, δ_s is the diffusive layer thickness, k_B is the Boltzmann constant, and T is the absolute temperature. Equation (3) can be written in the following variational form:

$$\int_S \nu_n\delta\nu_n dA=\int_S\{D\nabla_s^2\chi+\eta(\chi_0+\chi_\nu-\chi)\}\delta\nu_n dA, \tag{4}$$

where the integration is over the film surface. By assuming a symmetrical condition and applying the surface divergence theorem, we can rewrite Eq. (4) as

$$\int_S \nu_n\delta\nu_n dA=\int_S D\chi\nabla_s^2(\delta\nu_n)+\eta(\chi_0+\chi_\nu-\chi)\delta\nu_n dA. \tag{5}$$

This equation may be solved for ν_n using the finite-element method.

We choose u and ν as a set of curvilinear coordinates parametrizing the surface. The surface equation can be expressed by $\mathbf{r}(u,\nu)$. The surface gradient operator and surface Laplace operator can be expressed as[24]

$$\boldsymbol{\nabla}_s=\frac{1}{H^2}\mathbf{r}_1\left(G\frac{\partial}{\partial u}-F\frac{\partial}{\partial\nu}\right)+\frac{1}{H^2}\mathbf{r}_2\left(E\frac{\partial}{\partial\nu}-F\frac{\partial}{\partial u}\right) \tag{6}$$

and

$$\nabla_s^2=\frac{1}{H}\frac{\partial}{\partial u}\left(\frac{G\dfrac{\partial}{\partial u}-F\dfrac{\partial}{\partial\nu}}{H}\right)+\frac{1}{H}\frac{\partial}{\partial\nu}\left(\frac{E\dfrac{\partial}{\partial\nu}-F\dfrac{\partial}{\partial u}}{H}\right), \tag{7}$$

where partial derivatives with respect to u, ν are denoted by the use of the subscripts 1, 2 respectively; and $E=\mathbf{r}_1\cdot\mathbf{r}_1$, $F=\mathbf{r}_1\cdot\mathbf{r}_2$, $G=\mathbf{r}_2\cdot\mathbf{r}_2$, and $H^2=EG-F^2$.

NUMERICAL PROCEDURE

A finite-element method with a semi-implicit Euler scheme is introduced to solve Eq. (5). The reference surface configuration is perturbed by a small displacement u_n along the normal direction of the surface within a small time interval Δt. In the forward Euler numerical scheme, $u_n=\nu_n\Delta t$. The new surface configuration equation is

$$\mathbf{r}'=\mathbf{r}+u_n\mathbf{n}, \tag{8}$$

where $\mathbf{r}(u,\nu)$ and $\mathbf{r}'(u,\nu)$ are the surface reference configuration and the perturbed configuration, respectively, and $\mathbf{n}$ is the surface normal vector. The mean curvature after the perturbation is[24]

$$\kappa'=\kappa+\mathbf{n}\cdot\nabla_s^2(u_n\mathbf{n})-2\overline{\boldsymbol{\nabla}}\cdot(u_n\mathbf{n}), \tag{9}$$

where

$$\overline{\boldsymbol{\nabla}}=-\frac{1}{H^2}\mathbf{n}_1\left(G\frac{\partial}{\partial u}-F\frac{\partial}{\partial\nu}\right)+\frac{1}{H^2}\mathbf{n}_2\left(E\frac{\partial}{\partial\nu}-F\frac{\partial}{\partial u}\right) \tag{10}$$

is a surface operator. It can be proved that κ' can be simplified as

$$\kappa' = \kappa + \nabla_s^2 u_n + u_n(\kappa^2 - 2K), \tag{11}$$

where K is the Gaussian curvature. Replacing κ in Eq. (5) with κ' and rearranging the equation, we can write the semi-implicit scheme as

$$\begin{aligned}\int_S u_n \delta\nu_n + \Delta t \Omega \gamma [\nabla_s^2 u_n + u_n(\kappa^2 - 2K)] \\ \times (D\nabla_s^2 \delta\nu_n - g\delta\nu_n) dA \\ = \Delta t \Omega \int_S (\omega - \kappa\gamma)(D\nabla_s^2 \delta\nu_n - g\delta\nu_n) + g\chi_\nu \delta\nu_n dA.\end{aligned} \tag{12}$$

This equation may be solved for u_n using the finite-element method.

A finite-element method for computing the surface evolution of the film has been developed.[21] The geometry of the film surface is specified at time t. Our objective is to calculate the shape change of the surface during a subsequent infinitesimal time interval Δt. At time t, the stress and strain distribution along the surface is calculated to obtain the strain energy distribution on the surface. The calculation follows small-strain elastic theory. Next the surface curvature based on a rectangular mesh of nine Lagrangian elements on the surface is determined. Finally Eq. (12) is solved to obtain the surface displacement and a new surface during the time interval Δt. Based on the configuration at $t+\Delta t$, the new configuration during a subsequent infinitesimal time interval Δt is calculated. This process is repeated and the surface evolution is modeled.

The triangular plate bending element devised by Specht[25] was used to solve the surface diffusion. The plate element shape functions are parametrized by the three areal coordinates, L_1, L_2, and L_3. The local coordinates of the plate bending element, x, y, are chosen as the curvilinear coordinates. The following relations are used to transform the two coordinate systems:

$$\frac{\partial}{\partial x} = \frac{1}{2\Delta}\left(b_1\frac{\partial}{\partial L_1} + b_2\frac{\partial}{\partial L_2} + b_3\frac{\partial}{\partial L_3}\right), \tag{13}$$

$$\frac{\partial}{\partial y} = \frac{1}{2\Delta}\left(c_1\frac{\partial}{\partial L_1} + c_2\frac{\partial}{\partial L_2} + c_3\frac{\partial}{\partial L_3}\right), \tag{14}$$

where Δ is the area of the triangular element and

$$b_1 = y_2 - y_3, \quad b_2 = y_3 - y_1, \quad b_3 = y_1 - y_2,$$

$$c_1 = x_3 - x_2, \quad c_2 = x_1 - x_3, \quad c_3 = x_2 - x_1,$$

where (x_1, y_1), (x_2, y_2), and (x_3, y_3) are the nodal coordinates of the triangular element.

The following normalization scheme is used: $\omega_* = \omega/\omega_0$, $l_* = l/l_0$, $t_* = t/t_0$, where l is the length scale, t is the time scale, $\omega_0 = E\varepsilon_0^2/(1-\nu)$ is the strain energy density of the initially flat film, $l_0 = \gamma/\omega_0$, and $t_0 = \gamma^3/(\omega_0^4 D\Omega^2)$. Symmetrical boundary conditions are used in the calculations of strain energy density, surface curvatures, and surface evolution.

During Stranski-Krastanov growth, it is energetically unfavorable for the substrate to become exposed. To model this wetting effect, a thin transition layer with varied mismatch strain between the substrate and the fully strained film is introduced. The strain gradient is assumed to be linear. Physically, the transition region can be thought of as a mixed phase of the thin film and substrate, giving rise to the variation of the mismatch strain. An initial parametric study has shown that the surface evolution and island formation are insensitive to the transition layer thickness when its dimensionless thickness is less than 0.1. In the present simulations, the dimensionless transition layer thickness is taken as 0.1.

RESULTS AND DISCUSSION

The effects of growth rate on island formation and coarsening kinetics have been examined. A random perturbation in the form of a Fourier series with random amplitudes and wavelengths is introduced on the transition layer surface to mimic initial surface roughness. The computer simulations show that when the initial surface is random, the conclusions obtained in the present paper are insensitive to the starting configuration. During subsequent surface roughening and island formation, for simplicity, it is assumed that the variation of the surface chemical potential due to growth noise is much smaller than the variation of the total surface chemical potential. Hence, in subsequent growth, the small perturbation in the growth rate due to growth noise is neglected. As such, all of the simulations reported herein start from the same random surface. The dimensionless length and width of the simulation cells used are both 80, and the dimensionless substrate thickness is 16.

We focus on the situation close to complete condensation, i.e., the chemical potential of the vapor phase is larger than the surface chemical potential of the film, which is often the case in semiconductor growth. The growth parameter η_* is held fixed, which is equal to 5. The growth rate is controlled by the vapor chemical potential, $\chi_{*\nu}$. Three vapor chemical potentials are used during the simulation, i.e., $\chi_{*\nu} = 2$, 5, and 8, to represent low, intermediate, and high growth conditions, respectively. Also annealing has been simulated for a dimensionless film thickness of 0.2.

The snapshots of the surface morphology evolving during low, intermediate, and high growth rate, i.e., $\chi_{*\nu} = 2$, 5, and 8, are shown in Figs. 1, 2, and 3, respectively. These figures show that island formation and ripening kinetics are strongly affected by growth rate. At low growth rate, the rough surface evolves into flat and shallow islands, which subsequently evolve into isolated islands as shown in Fig. 1(a). The areal density of these isolated islands is relatively low. These islands start to undergo ripening at an earlier stage as shown in Fig. 1(b) compared with higher growth rates. As growth proceeds, larger islands grow at the expense of smaller islands as shown Fig. 1(c). Even at the later stage, islands remain sparsely distributed as shown in Fig. 1(d). At the intermediate growth rate, both islands and ripples appear at the early stage of evolution as shown Fig. 2(a). Subsequently, all the ripples break up into islands as shown in Fig. 2(b). The island density shown in Fig. 2(c) is higher than that

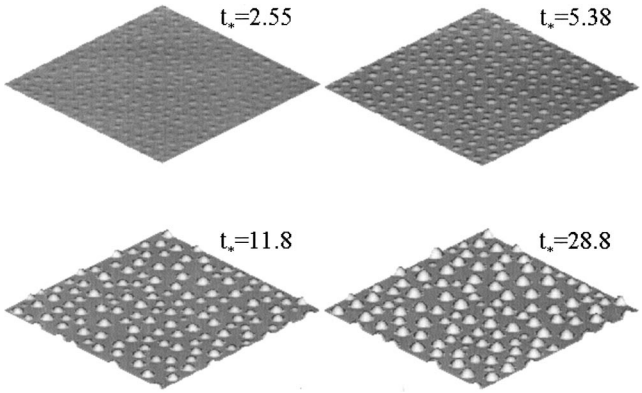

FIG. 1. Snapshots of surface morphologic evolution at low growth rate, that is, $\chi_{*\nu}=2$. (a) Isolated islands are formed with large separation; (b) islands undergo ripening at the earlier stage; as growth proceeds, the island density drops and the mean island volume increases as shown in (c) and (d).

of the low growth rate. As a result, the island separation becomes smaller. At the later stage, although the number of islands decreases, the coverage of the islands still increases as shown in Fig. 2(d). At high growth rate, both islands and ripples were observed as shown in Fig. 3(a). However, the number of ripples is higher than the number of islands. Subsequently, almost all of the ripples break up into islands [see Fig. 3(b)]. The mean island volume is larger than the previous two cases. The maximum island density is lower than that of the intermediate growth rate, but the island coverage is much higher as shown in Fig. 3(c). At the final stage, densely compact islands are formed as shown in Fig. 3(d). For the annealing case, a rippled structure is first formed as shown in Fig. 4(a). The rippled structure breaks up into islands [see Fig. 4(b)], followed by island ripening as shown in Fig. 4(c). As the ripening proceeds, the island density decreases [see Fig. 4(d)].

The evolution of the QD growth process can be divided into two stages: first, island formation, followed by island coarsening. In the simulations, coarsening starts at $t_* \approx 4$.

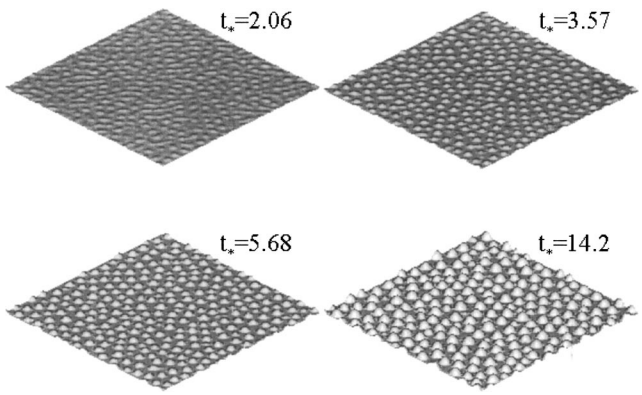

FIG. 2. Snapshots of surface morphologic evolution at intermediate growth rate, that is, $\chi_{*\nu}=5$. (a) Isolated islands and some ripples are formed; (b) ripples break up into islands; (c) islands undergo ripening, the island density drops, and the mean island volume increases; and (d) islands from a relatively dense array.

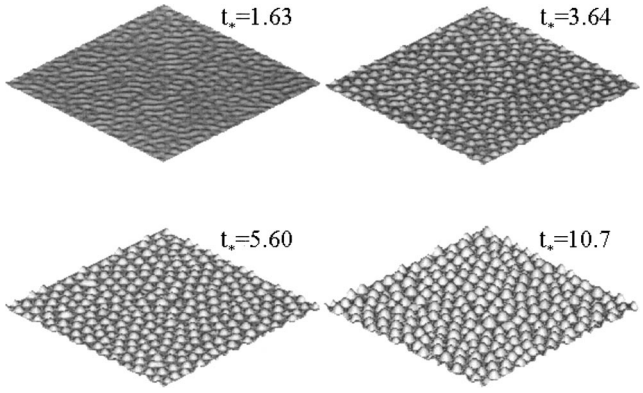

FIG. 3. Snapshots of surface morphologic evolution at high growth rate, that is, $\chi_{*\nu}=8$. (a) The formation of ripples is dominant; (b) ripples break up into islands; (c) islands undergo ripening, the island density drops, but the island coverage and the mean island volume increase; and (d) islands from a highly dense array.

From our simulations, some quantitative data on coarsening kinetics can be extracted. The mean island volume $\langle V_* \rangle$ versus growth time t_* is shown in Fig. 5 for the three growth cases and the annealing case. In the annealing case, the mean island volume increases linearly with growth time during coarsening. In the growth cases, the increase in mean island volume with respect to growth time is also approximately linear at low growth rate. However, with an increase of growth rate, the mean island volume increases more and more superlinearly with growth time, which is consistent with the unusual kinetics observed by Floro *et al.*[16]

The change in areal density of islands with respect to growth time for the three growth cases and the annealing case is shown in Fig. 6. During the early stage of coarsening, the areal density of islands $\langle N_* \rangle$ is shown to decrease at a higher-than-linear rate with growth time t_*. But with the increase of growth time, $\langle N_* \rangle$ decreases at a lower-than-linear rate. Interestingly, at high growth rates, the areal density of islands decreases almost linearly with growth time after the initial higher-than-linear regime. This result is consistent with the unusual coarsening kinetics.[16] In Fig. 6, the

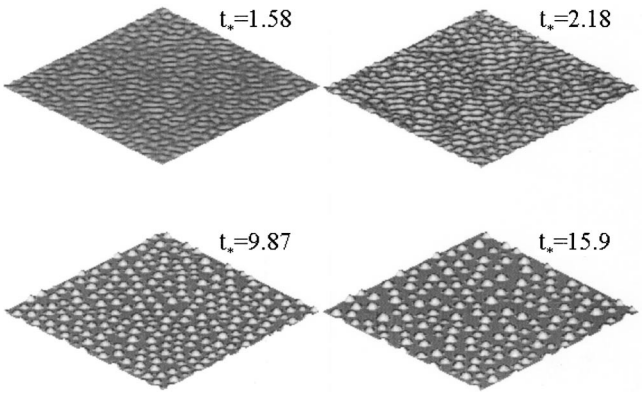

FIG. 4. Snapshots of surface morphologic evolution under annealing. (a) The formation of ripples is dominant; (b) ripples break up into islands; (c) islands undergo ripening, both the island density and the island coverage decrease, but the mean island volume increases; and (d) islands form a sparse array.

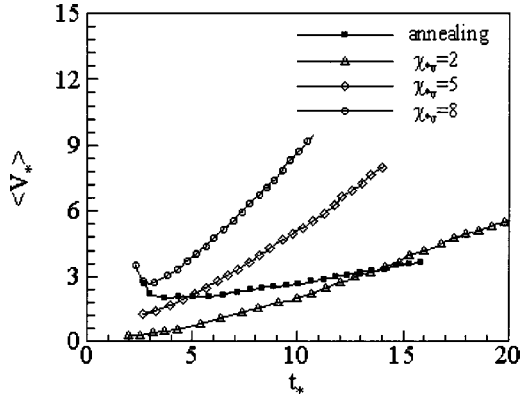

FIG. 5. The variation of the mean island volume $\langle V_* \rangle$ with growth time t_*. At the coarsening stage, the mean island volume increases superlinearly with time for the growth cases but linearly with time for the annealing case.

intermediate growth rate is shown to give rise to a maximum island density. This indicates that the maximum island density can be optimized by changing the growth rate.

The coverage of islands θ versus growth time t_* is shown in Fig. 7. In the annealed case, the coverage is shown to decrease linearly with growth time after island formation is completed. For the growth cases, the coverage increases linearly with time. This observation is different from the experimental results.[16] The reason for this difference is that in the experiment, the aspect ratio of islands is fixed since all islands adopt [501]-faceted surfaces. In the computer simulations, the islands adopt a nearly spherical cup shape since the surface energy is assumed to be isotropic. Figure 8 shows that the aspect ratio of islands increases with time, indicating the aspect ratio of the islands increases with increase of island volume.

It is interesting to note that the unusual coarsening kinetics observed by Floro *et al.*[16] also appears in the present simulations. Such unusual coarsening kinetics was attributed to the elastic interaction between the growing islands with

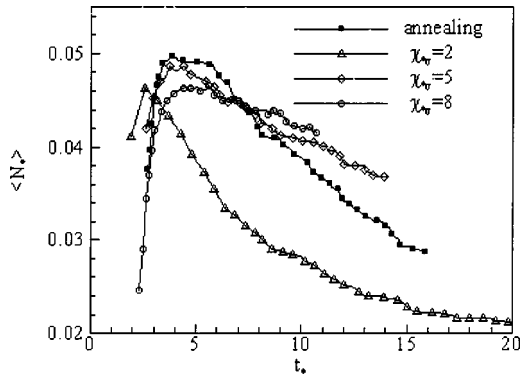

FIG. 6. The variation of the areal density of islands $\langle N_* \rangle$ with growth time t_*. At the initial growth and annealing stages, the areal density of islands increases drastically. At the early coarsening stage, $\langle N_* \rangle$ decreases at a higher-than-linear rate, while at the later stage, $\langle N_* \rangle$ decreases at a lower-than-linear rate. However, at high growth rate, $\langle N_* \rangle$ decreases close to a linear rate. For the annealing case, $\langle N_* \rangle$ decreases linearly with time.

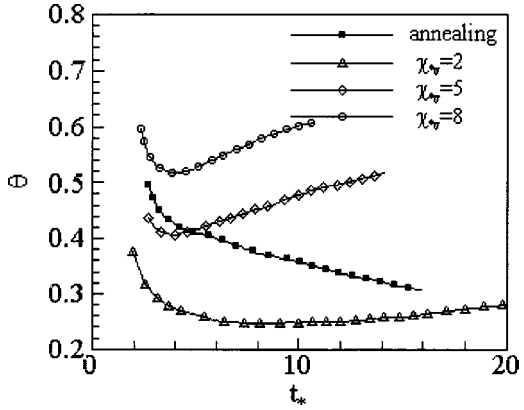

FIG. 7. The variation of the island coverage θ with time t_*. Since islands are shallow and flat at the early stage, the island coverage is high. As growth proceeds, the coverage first decreases and then starts to increase. For the annealing case, the coverage continues to decrease but in a slow pace. At the coarsening stage, the coverage changes linearly with time.

dense arrays.[16] In the present simulations, unusual kinetics is shown for sparse arrays of islands. This implies that the elastic interactions between islands may not be the only cause for unusual coarsening kinetics.

The island volume distributions at the beginning of coarsening are obtained and are shown in Fig. 9 for the three growth rates. These island size distributions are quite different from these observed in the nucleation mode. In the nucleation mode, the island size distribution was observed to follow a power-law decrease.[7] In addition, a uniform island size distribution was used to mimic the early stage of island coarsening.[26] In the present simulation, the island size distributions at the early stage of coarsening roughly follow a bell shape. The cause for the bell-shaped distribution is due to the inherent morphological instability of the strained film surface.[13,14] Through surface roughening, a rippled or cell-like corrugated surface pattern forms first, followed by the formation of islands. The surface roughening follows the

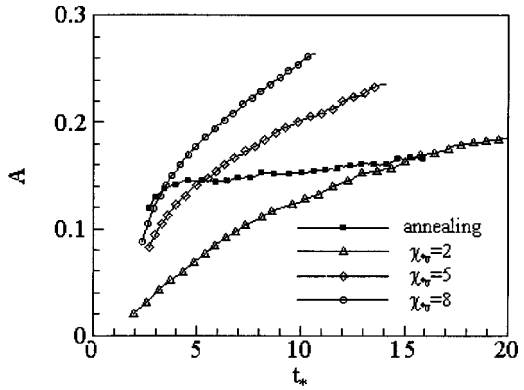

FIG. 8. The variation of island aspect ratio A with time t_*. At the initial growth and annealing stages, the aspect ratio A increases very quickly. At the coarsening stages, the aspect ratio A increases sublinearly with time for growth cases and linearly with time for the annealing case. The aspect ratio for the growth cases increases much faster than that for the annealing case.

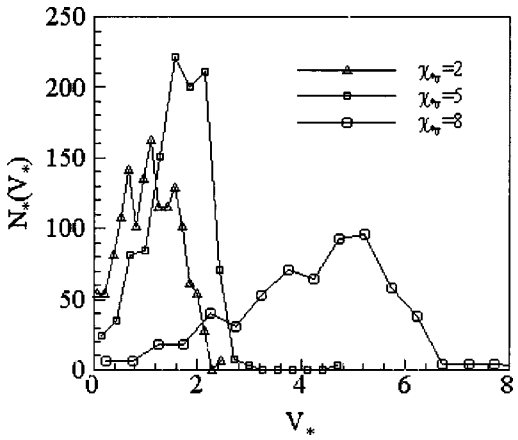

FIG. 9. The island volume distribution at the beginning of coarsening for the three growth cases.

characteristic roughening wavelengths. The fastest-roughening wavelength gives rise to the dominant surface roughening mode. The farther a roughening wavelength deviates from the fastest-roughening wavelength, the less dominant the corresponding surface roughening mode will be. Therefore a bell-shaped island distribution is developed with its peak corresponding to the fastest-roughening mode. In addition, the critical instability wavelength of the strained surface determines the smallest island volume, implying that there is a low bound for the island size. Based on the above analysis, the island size distributions shown in Figs. 9 and 11 should be usual for nucleationless island formation. It should be noted that the island distributions shown in Fig. 9 have also been observed experimentally. Examples include InAs/GaAs (Ref. 15) and Ge/Si(001) (Ref. 2) self-assembled coherent QD's. It is worth mentioning that the bell peak shifts towards to a larger value of volume when the growth rate is increased.

It is proposed that the unusual coarsening kinetics observed here could be attributed to the island size distribution at the beginning of coarsening. To validate this argument, the standard mean field theory used by Floro *et al.*[16] is employed to analyze the ripening kinetics during deposition and annealing. Following their formulation, the chemical potential is given as $\Delta\chi(V)=BV^{-1/3}$, where B denotes the energy scale and V denotes an island volume. The growth rate for any island of volume V is given by

$$\dot{V}=\frac{dV}{dt}=CV^{1/3}(e^{\Delta\chi_m/kT}-e^{\Delta\chi(V)/kT}), \tag{15}$$

where C is a constant, kT is as usual, and $\Delta\chi_m$ is specified by conservation of mass,

$$\int_0^\infty f(V,t)\dot{V}\,dV=\Phi, \tag{16}$$

where Φ is the deposition rate and $f(V,t)$ is the distribution of island volumes. The evolution of $f(V,t)$ is obtained from the flux continuity condition in size space,

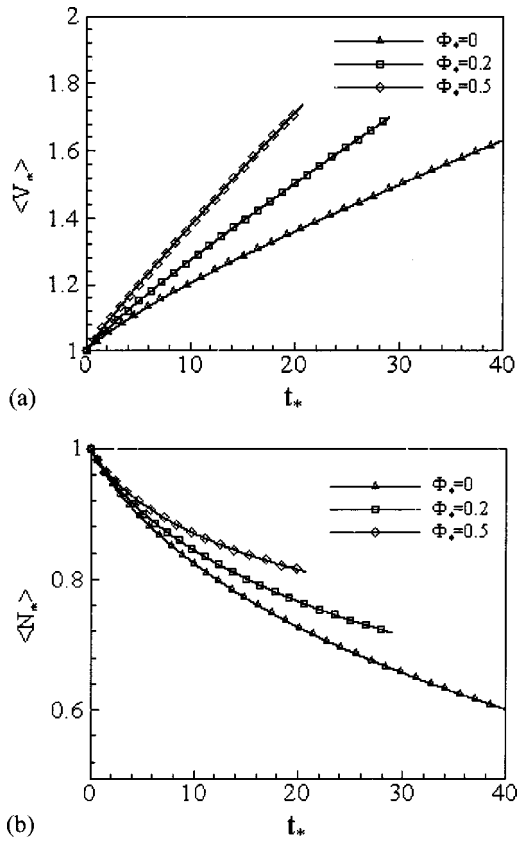

FIG. 10. When the island volume distribution follows a uniform distribution or a decreasing power-law distribution, the usual coarsening kinetics is observed. (a) The mean island volume changes sublinearly with time; (b) the areal density of islands decreases at a slower-than-linear rate (Φ_* is the growth flux).

$$\frac{\partial f}{\partial t}=-\frac{\partial(f\dot{V})}{\partial V}, \tag{17}$$

where the length scale is normalized by $l_0=B/kT$, the chemical potential by $\chi_0=kT$, and the growth time by $t_0=B^2/(Ck^2T^2)$. Equation (17) is solved numerically.

We use mean-field theory to study the effect of the island size distribution at the beginning of coarsening on the coarsening kinetics. If the island size distribution is uniformly distributed or follows a power-law decrease, the usual coarsening kinetics is obtained (see Fig. 10). However, if the initial island distributions follow a bell shape as shown in Fig. 11, the unusual coarsening kinetics is obtained (see Fig. 12). The underlying reason is that small islands exhibit a high chemical potential, which disappear more quickly than large islands. Since the number of small islands in the bell-shaped distribution is much less than that in the uniform or decreasing power-law distribution, the disappearing rate for small islands in the bell-shaped distribution should be much slower than that in a uniform or a decreasing power-law distribution, hence causing unusual coarsening kinetics.

In addition, unusual coarsening kinetics occurs even when the island density is sparse. This suggests that the elastic

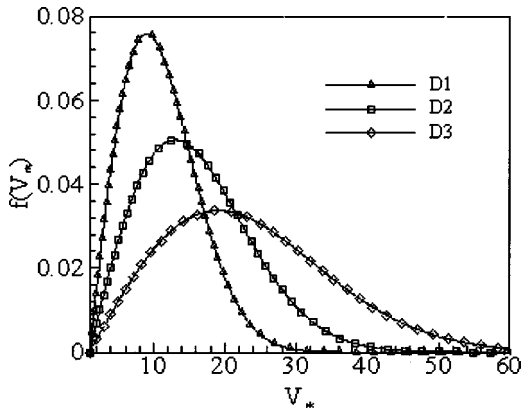

FIG. 11. Three bell-shaped island size distributions (denoted by D_1, D_2, and D_3, respectively).

interaction reasoning for growing islands with dense arrays may have a minor role compared to the initial bell-shaped island size distribution. It appears that the ''unusual'' kinetics is usual in nucleationless island formation since the bell-shaped island size distributions shown in Figs. 9 and 11 are not unusual in nucleationless island formation.

CONCLUSIONS

Large-scale three-dimensional computational studies of island formation and coarsening kinetics were performed. The computational results showed that the growth rate and growth mode play an important role in island formation and coarsening kinetics. Unusual island coarsening kinetics described by Floro *et al.*[16] was observed. Unusual coarsening kinetics is attributed to the bell-shaped island size distribution at the beginning of coarsening. The standard mean-field theory considering the initial island size distribution reproduces the unusual coarsening kinetics. Since the island size distribution at the early stage of nucleationless island formation is usual, it is proposed that the ''unusual'' coarsening kinetics is usual in the coarsening process with nucleationless island formation.

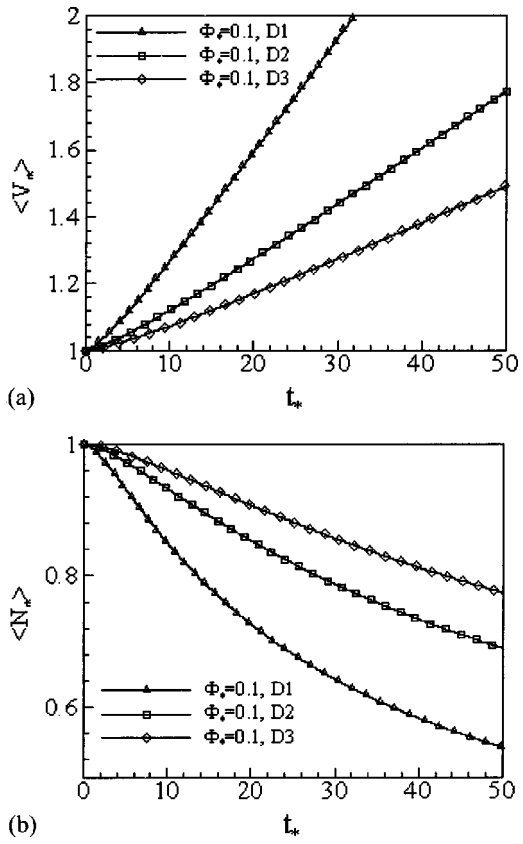

FIG. 12. When the bell-shaped island size distributions are used as the initial island distribution, unusual coarsening kinetics is observed. (a) The mean island volume changes superlinearly with time; and (b) the areal density of islands decreases at a higher-than-linear rate at the early stage of coarsening.

ACKNOWLEDGMENT

We express our gratitude to Dr. Julian Chia for proofreading the manuscript.

*Author to whom correspondence should be addressed. Electronic address: maszyw@nus.edu.sg

[1] D. Bimberg, M. Grundmann, and N. N. Ledentsov, Mater. Res. Bull. **23**, 31 (1998).
[2] I. Goldfarb, P. T. Hayden, J. H. G. Owen, and G. A. D. Briggs, Phys. Rev. B **56**, 10 459 (1997).
[3] R. M. Tromp, F. M. Ross, and M. C. Reuter, Phys. Rev. Lett. **84**, 4641 (2000).
[4] P. Sutter and M. G. Lagally, Phys. Rev. Lett. **84**, 4637 (2000).
[5] M. Zinke-Allmang, L. C. Feldman, S. Nakahara, and B. A. Davidson, Phys. Rev. B **39**, 7848 (1989).
[6] M. Goryll, L. Vescan, K. Schmidt, S. Mesters, H. Luth, and K. Szot, Appl. Phys. Lett. **71**, 410 (1997).
[7] N. Pino, R. Murri, and R. Rinaldi, Thin Solid Films **336**, 53 (1998).
[8] I. M. Lifshitz and V. V. Slyozov, J. Phys. Chem. Solids **19**, 35 (1961).
[9] B. K. Chakraverty, J. Phys. Chem. Solids **28**, 2401 (1967).
[10] B. K. Chakraverty, J. Phys. Chem. Solids **28**, 2413 (1967).
[11] L. Bardotti, M. C. Bartelt, C. J. Jenks, C. R. Stoldt, J. M. Wen, C. M. Zhang, P. A. Thiel, and J. W. Evans, Langmuir **14**, 1487 (1998).
[12] F. Family and P. Meakin, Phys. Rev. Lett. **61**, 428 (1988).
[13] R. J. Asaro and W. A. Tiller, Metall. Trans. **3**, 1789 (1972).
[14] M. A. Grinfeld, Dokl. Akad. Nauk (SSSR) **31**, 831 (1996) [Sov. Phys. Dokl. **31**, 831 (1986)].
[15] Y. Ebiko, S. Muto, D. Suzuki, S. Itoh, K. Shiramine, T. Haga, Y. Nakata, and N. Yokoyama, Phys. Rev. Lett. **80**, 2650 (1998).
[16] J. A. Floro, M. B. Sinclair, E. Chason, L. B. Freund, R. D. Twesten, R. Q. Hwang, and G. A. Lucadamo, Phys. Rev. Lett. **84**, 701 (2000).
[17] M. Krishnamurthy, J. S. Drucker, and J. A. Venables, J. Appl. Phys. **69**, 6461 (1991).
[18] L. Kuipers and R. E. Palmer, Phys. Rev. B **53**, R7646 (1996).

[19] C. Ratsch, A. Zangwill, P. Smilauer, and D. D. Vvedensky, Phys. Rev. Lett. **72**, 3194 (1994).
[20] J. Amar and F. Family, Phys. Rev. Lett. **74**, 2066 (1995).
[21] Y. W. Zhang and A. F. Bower, J. Mech. Phys. Solids **47**, 2273 (1999).
[22] Y. W. Zhang, Appl. Phys. Lett. **75**, 205 (1999).
[23] A. Pimpinelli and J. Villain, *Physics of Crystal Growth* (Cambridge University Press, Cambridge, 1997).
[24] C. E. Weatherburn, Quart. J. Pure Appl. Math. L , 230 (1925).
[25] B. Specht, Int. J. Numer. Methods Eng. **26**, 705 (1988).
[26] F. M. Ross, J. Tersoff, and R. M. Tromp, Phys. Rev. Lett. **80**, 984 (1998).